Computational insights into the structure of anhydrous Pu(III) oxalate

Sara B. Isbill[1*] and Andrew J. Miskowiec[1]

[1]1 Bethel Valley Road, Oak Ridge National Laboratory, Oak Ridge, TN, 37831 USA
[*]corresponding author: isbillsb@ornl.gov

Abstract

Despite the plutonium oxalate method's wide use in plutonium reprocessing, the method's mechanistic details remain unclear, particularly the identity of the plutonium oxidation state during conversion from an oxalate hydrate to the oxide. Recently, the optical vibrational spectra of Pu(III) oxalate during calcination were measured, providing an experimental reference for computational studies aimed at elucidating the oxalate structure. In this work, we compare the vibrational and electronic properties of two candidate anhydrous Pu(III) oxalate structures calculated using density functional theory with recent experiments. We find that both structures are plausible and may coexist at experimental temperatures, providing insights into the broad features measured in the Raman and infrared spectra.

Keywords

Plutonium oxalates, density functional theory, phonons, density of states

1. Introduction

Although the mechanistic details of the widely used plutonium oxalate method for plutonium reprocessing are still not precisely known, multiple oxidation states of plutonium are believed to participate in the oxalate calcination pathway [1-4]. Several factors complicate the elucidation of the plutonium oxalate to plutonium dioxide reaction mechanism, including the health and environmental safety challenges of working with plutonium. Existing studies clearly show that the intermediate reaction steps are dependent on the reaction environment. For example, slightly different reaction mechanisms have been reported for the decomposition of Pu(IV) oxalate under air or argon environments [1, 2]. Additionally, the oxidation state of the plutonium leads to differences in the hydration state and, subsequently, to changes in the thermal dehydration mechanism. Pu(III) oxalate stabilizes the nonahydrate with initial water loss occurring at 30°C–80°C, whereas Pu(IV) forms a hexahydrate with four waters removed during the first dehydration step at 60°C–100°C [1-3]. Several of the intermediates during the conversion of Pu oxalates to PuO_2 have not been isolated, prohibiting full characterization of the species, including their structure.

Christian et al. recently published a pair of complementary calcination studies [5, 6] of Pu(III) and Pu(IV) oxalates from their hydrated states—$Pu_2(C_3O_4)_3 \cdot 9H_2O$ and $Pu(C_3O_4)_2 \cdot 6H_2O$, respectively—to PuO_2. In their studies, the authors characterized samples after calcination at various temperatures via powder X-ray diffraction, Raman spectroscopy, and infrared (IR) spectroscopy. They noted several key differences between the Pu(III) and Pu(IV) calcination experiments. Significantly, interpretation of the Raman spectra at the intermediate temperatures of 250°C and 300°C for Pu(III) was precluded because substantial fluorescence was observed, and low-frequency features of the 160°C and 200°C samples were broad [5]. No such fluorescence or peak broadening was observed during Pu(IV) calcination [6]. Also, powder X-ray diffraction measurements of Pu(III) oxalate calcined to 160°C or higher showed amorphous patterns, whereas Pu(IV) oxalate had amorphous patterns only at temperatures of 220°C and 250°C [5, 6].

The studies of Christian et al. reveal that similar but distinct dehydration pathways occur for Pu(III) and Pu(IV) oxalates, and the atomic and electronic structural differences of the two pathways can likely inform the decomposition mechanism. Density functional theory (DFT) calculations can provide valuable insights into the dehydration pathway; however, the crystal structures of species along the Pu oxalate method pathway are not known, and several computational studies investigating possible Pu oxalate structures exists. Garrett et al. investigated the structure of $Pu(C_3O_4)_2 \cdot 6H_2O$, starting with the known structure of the uranium analogue [7], and South and Roy performed an energetic investigation into candidate anhydrous Pu(III) and Pu(IV) oxalate structures using other actinide analogues and the hydrated structures as starting points [8]. We previously extended the energetic study of South and Roy for anhydrous Pu(IV) oxalate to include structural stability via phonon analysis, revealing only one of the two candidate structures was stable [9]. The symmetry of the phonon modes was analyzed to determine predicted optical activity, and the frequency of optically active modes was compared with the peak frequencies reported by Christian et al. [6], showing that the stable anhydrous structure was also predicted to have a Raman mode in excellent agreement with an experimentally measured Raman peak.

We now aim to complete a similar investigation for the candidate anhydrous Pu(III) oxalates in light of Christian et al.'s recent study of Pu(III) decomposition [5]. In this work, we perform DFT investigations into the structure, phonons, and electronic density of states of two candidate $Pu_2(C_2O_4)_3$ structures taken from the literature. We connect our work to recent experimental studies and provide support for the broad features observed in the Raman, IR, and powder X-ray diffraction measurements made for Pu(III) oxalates. We also provide the calculated electronic density of states to rationalize the experimentally observed fluorescence at intermediate temperatures. This work takes another step toward understanding the mechanistic details of the Pu oxalate method that have eluded scientific confirmation for 80 years.

2. Computational methods

We performed DFT relaxation and phonon calculations of two candidate anhydrous Pu(III) oxalate structures taken from South and Roy [8]. These structures are referred to as ox-1 and ox-2, consistent with the nomenclature used in the South and Roy work [8]. The initial structures were relaxed using the Vienna ab initio Simulation Package (VASP 6.2.1) [10-12] with the PBEsol exchange-correlation function [13], van der Waals DFT-D3 corrections by Grimme et al.

[14], and a 900 eV cutoff energy in an antiferromagnetic (AFM) configuration [7, 8] using the regular Projector-Augmented Wave potentials provided with VASP for each atomic species [15, 16]. The relaxations were performed in two steps. First, the structures were relaxed until forces were less than 0.01 eV/Å using a Γ-centered *k*-point mesh with a spacing of 0.3 $Å^{-1}$ between *k*-points. The structures were then further relaxed using a denser *k*-point mesh, where the spacing was 0.14 $Å^{-1}$. These *k*-spacings resulted in 10–14 *k*-points for the ox-1 structure at the 0.3 $Å^{-1}$ spacing, owing to a large volume change during the relaxation and 104 *k*-points at the 0.14 $Å^{-1}$ spacing. For the ox-2 structure, the 0.3 and 0.14 $Å^{-1}$ spacings resulted in 10 and 80 *k*-points, respectively. During geometry relaxation, the electronic structure was described using Gaussian smearing with a smearing width of 0.1 eV and an energy convergence value of 1×10^{-8} eV. A final single point energy calculation was performed on the relaxed structures using the tetrahedron method with Blöchl corrections and a 0.10 $Å^{-1}$ *k*-spacing, resulting in 225 and 185 *k*-points for ox-1 and ox-2, respectively [17]. All *k*-point spacings were selected based on convergence testing to balance accuracy in the electronic energy for different aspects of the calculation (relaxation versus single point energy calculation) with computational cost. The electronic density of states was calculated using a dense 8,000-point grid from the self-consistent charge density calculated in the final single point energy calculation. Based on several previous reports for similar systems, an effective Hubbard +U correction of 4.0 eV using the method of Dudarev et al. [18] was applied to the plutonium centers to break the degeneracy of the 5*f* electrons [7, 19, 20].

Phonons were calculated for the final structures using the finite displacement method as implemented in Phonopy [21]. Displacements were determined using the default symmetry tolerance in Phonopy. $20 \times 20 \times 20$ and $14 \times 14 \times 14$ meshes were used with a frequency sampling pitch of 1.0 cm^{-1} for ox-1 and ox-2, respectively, to calculate the phonon density of states.

3. Results

3.1. Relaxed structures

The initial structures are taken from the work of South and Roy [8] and relaxed to tighter force and energy convergence values for extension to phonon analysis. The relaxed structures are shown in Fig. 1. During relaxation, the ox-1 structural parameters changed significantly, as detailed in Table 1. The final ox-1 volume was nearly half the initial volume, mostly through significant reduction of the *a* lattice parameter, although non-negligible changes to the *b* and *c* lattice parameters were also calculated. This large change in volume likely arises from the different DFT parameters used in this work compared to that of South and Roy, suggesting the previously identified ox-1 structure may have been a metastable structure. Minor changes were also observed for the ox-2 structure, though the volume only increased by approximately 4%. Despite the changes to the lattice parameters, both systems retained $P2_1/c$ symmetry.

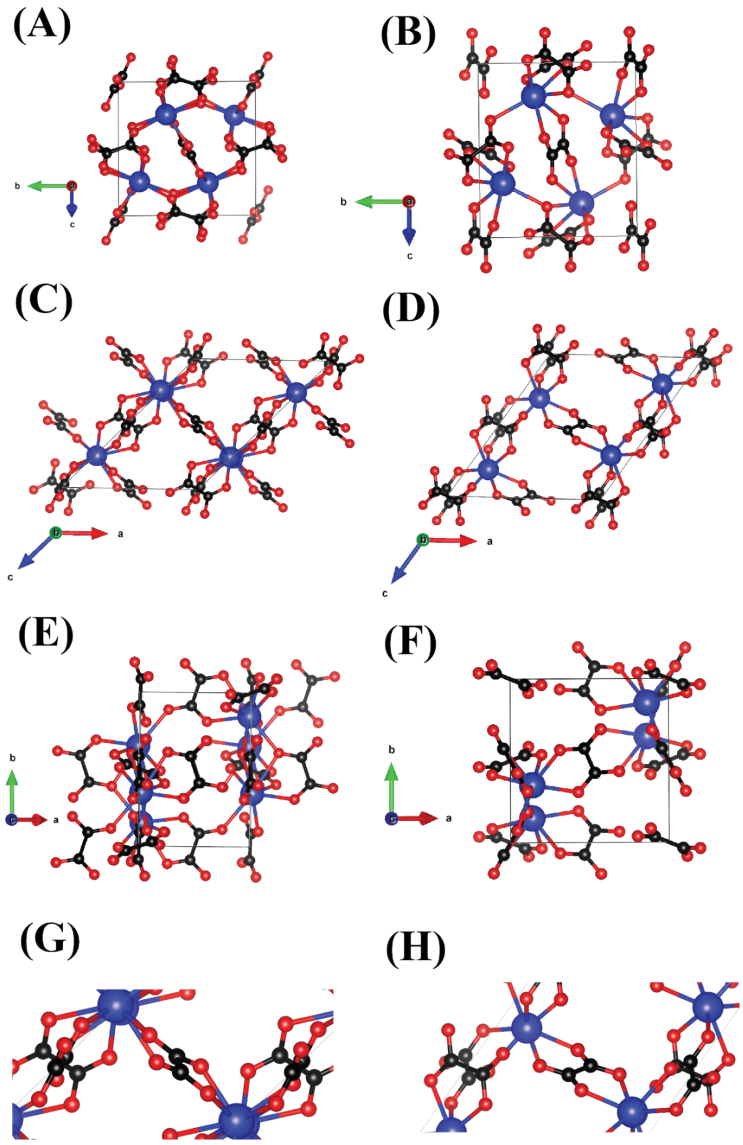

Fig. 1. Relaxed ox-1 (A, C, E, G) and ox-2 (B, D, F, H) structures viewed along *a* (A, B), *b* (C, D), and *c* (E, F) lattice directions. A close-up of the oxalate coordination when viewed along *b* is given in panels G and H.

Table 1. Cell parameters. Initial and final unit cell parameters and electronic structure for ox-1 and ox-2 structures. Initial structural parameters are taken from Ref [8].

Parameter	ox-1 initial	ox-1 final	ox-2 initial	ox-2 final
a **(Å)**	11.90	8.47	9.88	9.41
b **(Å)**	9.88	8.34	8.26	8.02
c **(Å)**	10.4	11.51	9.50	10.76
α (°)	90.0	90.0	90.0	90.0
β (°)	119.0	135.0	123.6	124.3
γ (°)	90.0	90.0	90.0	90.0
vol (Å^3)	1069.4	575.2	645.5	670.4

Energy (eV/atom)	--	−9.066	--	−9.048
Band gap (eV)	--	2.470	--	2.232
Space group	$P2_1/C$ (14)	$P2_1/C$ (14)	$P2_1/C$ (14)	$P2_1/C$ (14)

Although the final volume of ox-1 is approximately 100 $Å^3$ less than that of ox-2, the final relaxed structures are quite similar, with the main difference being rotation of the oxalate ligands (compare, for example, Fig. 1C and Fig. 1D). It is also worth noting that in the ox-1 structure, the plutonium atoms lie on the edge of the unit cell and are coplanar when viewed down the *b* lattice vector (Fig. 1E). In ox-2, however, the plutonium atoms sit just within the edge of the unit cell and are no longer coplanar (Fig. 1F). The nearest neighbor Pu-Pu distances are 4.18, 5.98, and 6.22 Å in ox-1 and 4.55, 5.62, and 6.10 Å in ox-2. The shortest Pu-Pu distance lies along the *b* lattice direction. This distance is shorter in ox-1 than in ox-2 because of the coplanarity of the Pu atoms when viewed down the *b* lattice in this structure. When the Pu atoms are shifted off the edge of the unit cell as they are in ox-2, the Pu-Pu distance along the perpendicular direction (the *b* lattice) increases. The intermediate Pu-Pu distance is along the *c* lattice vector. This distance is shorter in ox-2 owing to the shorter *c* lattice vector in ox-2 than in the ox-1 structure. The third Pu-Pu distance arises where the atoms lie in different planes along the *b* and *c* lattices.

3.2. Electronic structure

The relative electronic energy difference between the relaxed ox-1 and ox-2 structures is 0.719 eV or 0.018 eV/atom (208 K). This result is consistent with thermal energy at room temperature, indicating that at temperatures high enough to dehydrate the oxalate, both structures are energetically accessible and could coexist based on the thermodynamics. We have not pursued a kinetics investigation that would provide information about any energetic barriers to formation for the two candidate structures; however, at several intermediate temperatures studied by Christian et al. [5], an amorphous X-ray diffraction pattern was measured, revealing no long-range crystalline order in the experimental system. This experimental finding does not contradict the possible coexistence of structures.

Several features in the electronic density of states (eDOS), given in Fig. 2, are worth discussing. First, we have modeled the AFM magnetic structure, which results in the up- and down-spin channels being nearly identical. LaCount et al. investigated the AFM and ferromagnetic structures of hydrated plutonium oxalates using DFT+U and found that the geometries were nearly identical; in the case of the Pu(III) oxalate, the energy difference between the two structures was only 0.1 meV per formula unit [22]. The AFM structure has also been used in other DFT studies of Pu(III) oxalates [8]. Fig. 2 shows minor differences in the intensity of the up- and down-spin channels in the total eDOS, but the differences are negligible.

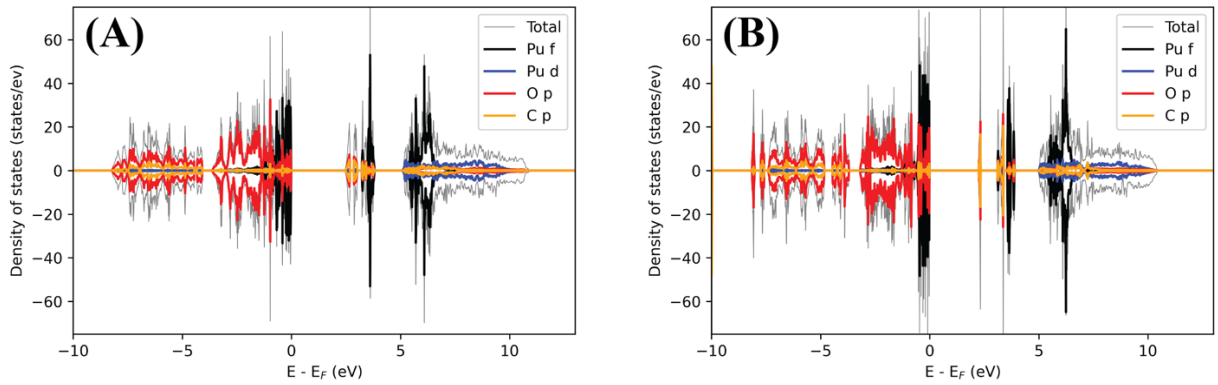

Fig. 2. Electronic density of states of ox-1 (A) and ox-2 (B). The calculated band gaps are 2.470 and 2.232 eV for ox-1 and ox-2, respectively. The up-spin channel is given positive density of states values, and the down-spin channel is depicted with negative density of states values.

Second, both structures show semiconducting electronic behavior with band gaps of 2.470 and 2.232 eV for ox-1 and ox-2, respectively. These band gaps correspond to approximately 500 and 553 nm. Christian et al. [5] observed strong fluorescence at 250 and 300 °C with a 514-nm laser which, disregarding considerations of parity conservation, is not inconsistent with the electronic band gap calculated for the ox-1 and ox-2 structures here. Thus, the predicted band gaps are not too large to suppress fluorescence; however, experimental measurements are needed to verify the calculated band gaps. Secondary gaps are also seen for each structure approximately 3.8 eV above the Fermi energy. These gaps are 1.269 and 1.101 eV for ox-1 and ox-2, respectively. The ox-2 structure contains a non-negligible intermediate gap of 0.763 eV after the first conduction band of O *p* and C *p* character that is absent in ox-1.

Third, almost all the calculated eDOS bands are very sharp, indicating the electronic dispersions are likely very flat across the Brillouin zone, implying spherical symmetry. The Pu *d* orbitals are unoccupied and therefore do not participate in bonding. Because no Pu *d* orbitals are available for bonding, the Pu-O bonding is primarily between the Pu *f* orbitals and the O *p* orbitals. Additionally, the O-C bonding is between the *p* orbitals on the O and C atoms. The lowest-energy conduction bands are O *p* and C *p* in character, though the Pu *f* conduction bands appear before the large secondary gap in each structure. The Pu *d* orbitals are found after the secondary gap in both structures.

3.3. Phonons

For comparison with recent experiments, the phonon band structure and phonon density of states were calculated for both relaxed structures and are shown in Fig. 3. Although neither system contains significant imaginary modes at the Γ point, minor imaginary modes are observed between some high-symmetry points in the irreducible Brillouin zone. Specifically, ox-1 has a small imaginary band between Y and Γ, and ox-2 has a small imaginary band between Γ and B. Both structures also have small imaginary bands between Γ and Z.

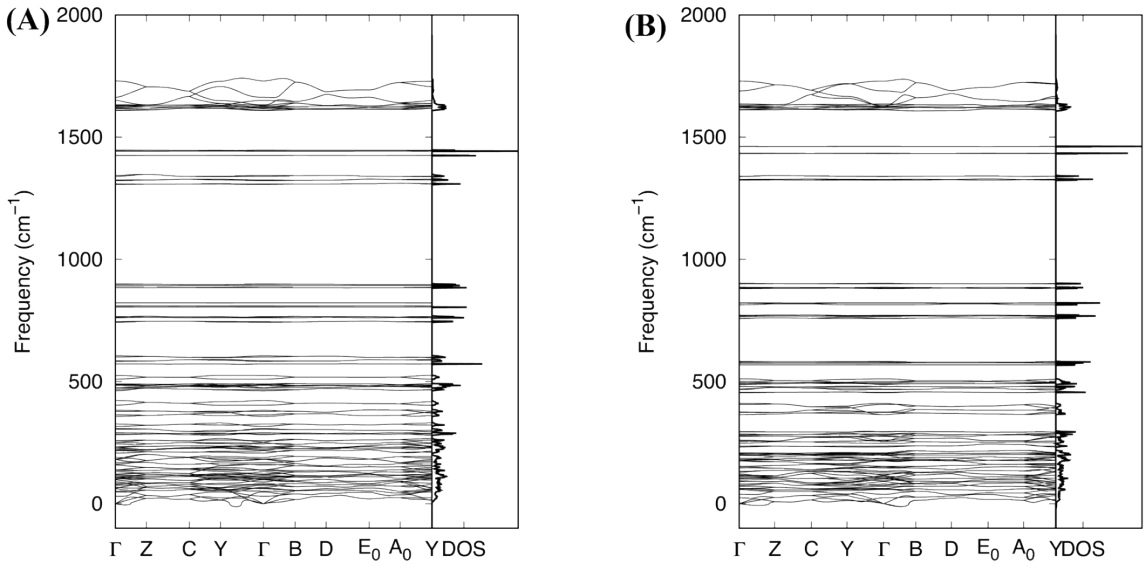

Fig. 3. Phonon band structure and phonon density of states for ox-1 (A) and ox-2 (B).

Most of the bands are flat across the irreducible Brillouin zone, and only minor differences are observed between the two structures owing to their similar symmetry and bond lengths. Because the symmetry of the structures is low, all modes are predicted to be either Raman or IR active. However, some bands have appreciable dispersion above 1500 cm^{-1}. Inspection of the eigenvectors reveals these modes are in-plane stretches of the oxalate ligands. The oxalate ligands are oriented along several different crystallographic directions (Fig. 1), and this structural anisotropy manifests in distinct phonon frequencies for similar oxalate vibrational modes oriented along different crystallographic planes. Fig. 4 shows an example of this behavior at Γ. Two modes, differing by only 2 cm^{-1}, show in-plane oxalate stretching modes, though only one of the modes contains displacements for oxalate ligands oriented along the *a* lattice.

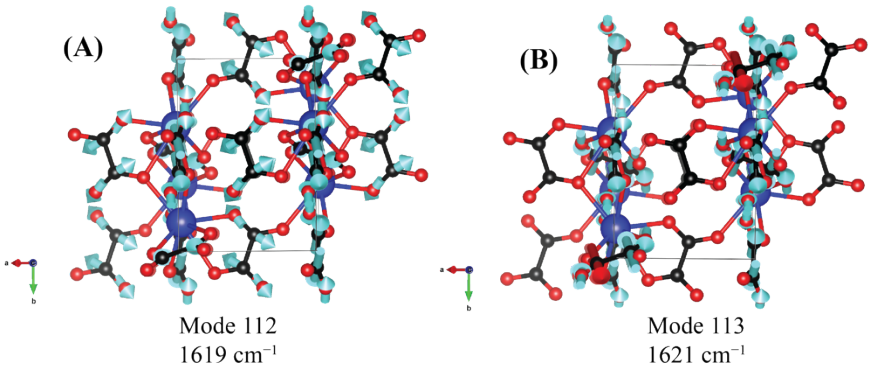

Fig. 4. Eigenvectors of two phonon modes in ox-1 at Γ. The mode at 1619 cm^{-1} (A) shows displacement for atoms along the *a* lattice direction, whereas the mode at 1621 cm^{-1} (B) does not. Both modes show atomic displacements for atoms along the *c* lattice direction.

4. Discussion

The ox-1 and ox-2 structures considered in this work were found to be similar in all aspects investigated. The calculated electronic band gaps are comparable, differing by only 0.238 eV. Additionally, the electronic energies differ by only 0.018 eV/atom (208 K), suggesting the slightly higher-energy ox-2 structure could be accessible at the experimental temperatures. Extension of the energetic comparison to Gibbs free energy using the thermal properties tags in Phonopy confirmed that the energetic differences between the two candidate structures are substantially less than the available thermal energy across the entire experimental temperature range in the work of Christian et al. [5], as shown in Fig. 5. However, the free energy of the species become negative (stable) around 340 °C. From experimental powder X-ray diffraction and thermogravimetric analysis, conversion to PuO_2 occurs before 250 °C [1, 5]. The present work indicates the anhydrous species is unstable at such low temperatures which may explain why anhydrous Pu(III) oxalate has not been experimentally isolated.

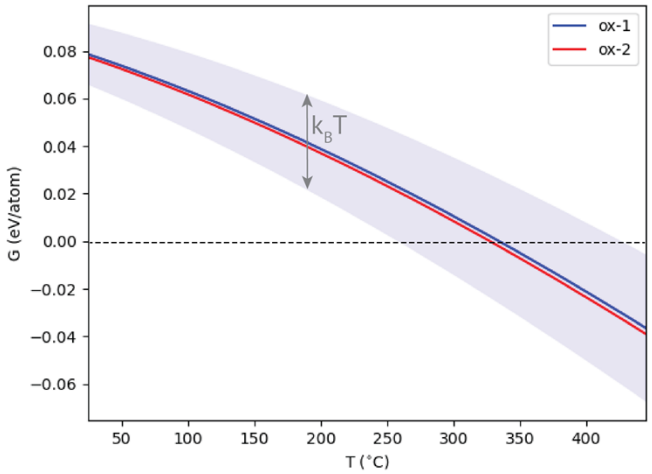

Fig. 5. Gibbs free energy analysis of ox-1 and ox-2. The shaded region denotes thermal energy at each temperature, and the dashed horizontal line denotes the divide between unfavorable (positive) and favorable (negative) free energy.

Additionally, both Pu(III) structures investigated have equal stability based on the phonon band structures; neither structure contains large imaginary modes, and small imaginary bands are only observed away from Γ. Investigation of the eigenvectors in ox-1 reveals two modes that may cause the transformation of ox-1 to ox-2. These modes (Fig. 6) are found at 115 and 130 cm^{-1}, equivalent to 0.014 eV (162 K) and 0.016 eV (185 K), respectively, further indicating that coexistence of the modes is plausible at the experimental temperatures. Because both structures are reasonable from a thermodynamic perspective, additional kinetics investigations beyond the scope of the present work would be necessary for additional insight into the likely formation of each structure during dehydration.

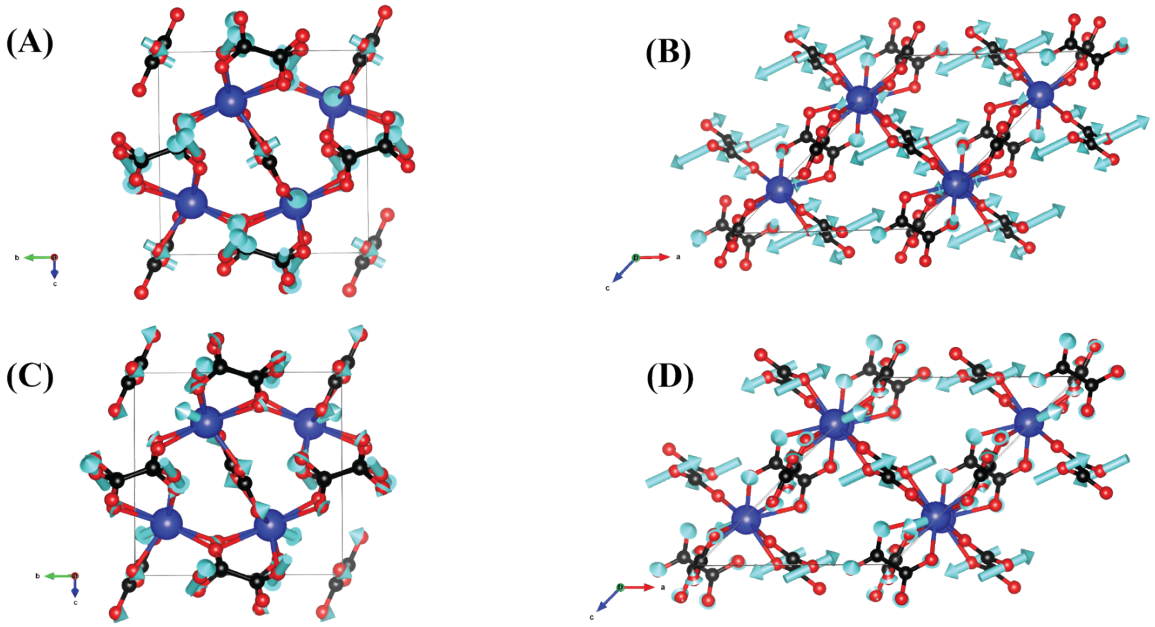

Fig. 6. Eigenvectors of mode 21 (A, B) and mode 24 (C, D) of ox-1 at Γ along the *a* (A, C) and *b* (B, D) lattice directions. The calculated frequencies of modes 21 and 24 are 115 and 130 cm^{-1}, respectively.

The primary differences between the ox-1 and ox-2 structures in this work are rotation of the oxalate ligand and shift of the Pu atoms. Although it may seem intuitive that such minor structural changes would not induce large electronic or vibronic changes, we previously found significant changes arising from similar structural distortions in our investigation of the Pu(IV) oxalate [9]. In that work, we investigated the vibrational properties of two candidate anhydrous Pu(IV) oxalate structures. The oxalate rotational modes observed for the first Pu(IV) structure had a non-negligible imaginary frequency (−52 cm^{-1}) at Γ. This is contrasted by the oxalate rotational modes in Pu(III) with low, real frequencies (Fig. 6). Additionally, we identified a unique phonon mode near 1380 cm^{-1} in the second Pu(IV) oxalate structure (which was absent in the first structure), related to the oxalate stretch; this mode was in excellent agreement with an experimentally measured Raman peak [6]. Therefore, we were able to support the presence of the second candidate structure in the experimental Pu(IV) oxalate calcination pathway.

Although our present findings for anhydrous Pu(III) oxalate cannot provide direct support for structure(s) present in the experimental calcination pathway, our work still supports recent experimental data in multiple ways. First, both structures could plausibly lead to the experimentally observed fluorescence at intermediate temperatures owing to the modest band gaps of 2.232 to 2.470 eV because most common laser wavelengths would be able to excite an electron across the gap to a conduction band rather than to a virtual state within the band gap [5]. Second, our findings are consistent with many of the broad patterns and spectra measured by Christian et al. [5] during the calcination of Pu(III) oxalate to PuO_2. Experimentally, the broad powder X-ray diffraction patterns were attributed to amorphous structures during the dehydration reaction and low bulk crystallinity or disorder near the anhydrous composition [5]. Additionally, the Raman and IR spectra at several intermediate temperatures were broad, obscuring the resolved features measured at the low and high temperatures of their study [5]. Our work

suggests the broad features measured experimentally by Christian et al. may arise from the coexistence of multiple structures or disorder of the oxalate rotational coordination [5]. Although the atomic structures of ox-1 and ox-2 found in this work are similar, their volume and lattice parameters are distinct. The coexistence of these two structures, and possibly others, would appear as disorder when probed by powder X-ray diffraction. While not investigated in the present work, it is also possible that the kinetic barrier to oxalate rotation is low and the oxalate ligands can assume rotated and unrotated coordination in an individual crystal. Because the rotational state of the ligand affects the Pu-Pu distances and volume of the unit cell, amorphous features in the powder X-ray diffraction patterns are expected if more than one rotational state is present. Additionally, the variation in bond lengths would shift the phonon frequencies, broadening the Raman and IR peaks, again consistent with the findings of Christian et al. [5].

5. Conclusions

To provide additional insights into the structure of anhydrous Pu(III) oxalate by leveraging recent experimental work, we performed DFT calculations for two candidate Pu(III) oxalate structures. Unlike in the Pu(IV) oxalate case we investigated previously, we are not able to provide strong evidence in support of a single geometry as a stable anhydrous Pu(III) oxalate; rather, our findings indicate multiple closely related anhydrous structures may coexist and therefore provide possible explanations for the origin of broad features in recent X-ray diffraction patterns and Raman and IR spectra.

Our results are in qualitative agreement with recent experiments, but we note that another lower-energy stable geometry for anhydrous Pu(III) oxalate may exist. A thermodynamic investigation of possible Pu oxalate structures, such as this work, lays a foundation for further kinetics studies, which may provide additional insights into the plutonium oxalate to plutonium oxide mechanism. For example, a detailed kinetics investigation into the activation barrier for ox-1 to ox-2 transformation and the energetic barriers for the structural rearrangements associated with redox of the Pu center would add additional reference points to the potential energy landscape probed in this work, which may aid in a full understanding of the Pu oxalate method.

Acknowledgements

This research used resources of the Oak Ridge Leadership Computing Facility, which is a US Department of Energy Office of Science User Facility at Oak Ridge National Laboratory supported under Contract DE-AC05-00OR22725. This work was supported by the National Nuclear Security Administration.

References

1. De Almeida, L., et al., *Insights into the Thermal Decomposition of Lanthanide(III) and Actinide(III) Oxalates – from Neodymium and Cerium to Plutonium.* Europ. J. Inorg. Chem., 2012. **2012**(31): p. 4986-4999. 10.1002/ejic.201200469
2. Vigier, N., et al., *Reaction mechanisms of the thermal conversion of Pu(IV) oxalate into plutonium oxide.* J. Alloys Comp., 2007. **444-445**: p. 594-597. 10.1016/j.jallcom.2007.01.057

3. Orr, R.M., H.E. Sims, and R.J. Taylor, *A review of plutonium oxalate decomposition reactions and effects of decomposition temperature on the surface area of the plutonium dioxide product.* J. Nucl. Mater., 2015. **465**: p. 756-773. 10.1016/j.jnucmat.2015.06.058
4. Kartushova, R.E., T.I. Rudenko, and V.V. Fomin, *Thermal decomposition of tetravalent and trivalent plutonium oxalates.* Soviet J. At. Energy, 1958. **5**: p. 831-835.
5. Christian, J.H., et al., *Probing the thermal decomposition of plutonium (III) oxalate with IR and Raman spectroscopy, X-ray diffraction, and electron microscopy.* J. Nucl. Mater., 2023. **584**: p. 154596. 10.1016/j.jnucmat.2023.154596
6. Christian, J.H., et al., *Raman and infrared spectra of plutonium (IV) oxalate and its thermal degradation products.* J. Nucl. Mater., 2022. **562**: p. 153574. 10.1016/j.jnucmat.2022.153574
7. Garrett, K.E., et al., *First principles investigation of the structural and bonding properties of hydrated actinide (IV) oxalates, $An(C_2O_4)_2{\cdot}6H_2O$ (An = U, Pu).* Comput. Mater. Sci., 2018. **153**: p. 146-152. 10.1016/j.commatsci.2018.06.033
8. South, C.J. and L.E. Roy, *Insights into the thermal decomposition of plutonium(IV) oxalate – a DFT study of the intermediate structures.* J. Nucl. Mater., 2021. **549**. 10.1016/j.jnucmat.2021.152864
9. Isbill, S.B., et al., *Computational insights into the lattice dynamics of Pu(IV) oxalates.* J. Nucl. Mater., 2023. **573**: p. 154106. 10.1016/j.jnucmat.2022.154106
10. Kresse, G. and J. Hafner, *Ab initio molecular dynamics for liquid metals.* Phys. Rev. B 1993. **47**(1): p. 558-561. 10.1103/physrevb.47.558
11. Kresse, G. and J. Furthmüller, *Efficient iterative schemes for ab initio total-energy calculations using a plane-wave basis set.* Phys. Rev. B, 1996. **54**(16): p. 11169.
12. Kresse, G. and J. Furthmüller, *Efficiency of ab-initio total energy calculations for metals and semiconductors using a plane-wave basis set.* Comput. Mater. Sci., 1996. **6**: p. 15-50.
13. Csonka, G.I., et al., *Assessing the performance of recent density functionals for bulk solids.* Physical Review B, 2009. **79**(15). 10.1103/PhysRevB.79.155107
14. Grimme, S., et al., *A consistent and accurate ab initio parametrization of density functional dispersion correction (DFT-D) for the 94 elements H-Pu.* J Chem Phys, 2010. **132**(15): p. 154104. 10.1063/1.3382344
15. Blochl, P.E., *Projector augmented-wave method.* Phys. Rev. B 1994. **50**(24): p. 17953-17979. 10.1103/physrevb.50.17953
16. Kresse, G. and D. Joubert, *From Ultrasoft Pseudopotentials to the Projector Augmented-Wave Method.* Phys. Rev. B, 1999. **59**: p. 1758-1775.
17. Blöchl, P.E., O. Jepsen, and O.K. Andersen, *Improved tetrahedron method for Brillouin-zone integrations.* Phys Rev B, 1994. **49**(23): p. 16223-16233. 10.1103/physrevb.49.16223
18. Dudarev, S.L., et al., *Electron-energy-loss spectra and the structural stability of nickel oxide: An LSDA+U study.* Phys. Rev. B, 1998. **57**: p. 1505-1509.
19. Wen, X.-D., et al., *A Screened Hybrid DFT Study of Actinide Oxides, Nitrides, and Carbides.* The Journal of Physical Chemistry C, 2013. **117**(25): p. 13122-13128. 10.1021/jp403141t
20. Yang, R., et al., *Hybrid density functional study on lattice vibration, thermodynamic properties, and chemical bonding of plutonium monocarbide.* Chinese Physics B, 2016. **25**(6). 10.1088/1674-1056/25/6/067106

21. Togo, A., L. Chaput, and I. Tanaka, *Distributions of phonon lifetimes in Brillouin zones.* Phys. Rev. B, 2015. **91**(9): p. 094306. 10.1103/PhysRevB.91.094306
22. LaCount, M.D., et al., *Ab initio modeling and thermodynamics of hydrated plutonium oxalates.* Journal of Nuclear Materials, 2023. **583**: p. 154504. 10.1016/j.jnucmat.2023.154504